

# Complexity of emerging magnetic flux during lifetime of solar ephemeral regions

Hanlin Yang 

Key Laboratory of Solar Activity and Space Weather, National Astronomical Observatories, Chinese Academy of Science, Beijing 100101, People's Republic of China  
University of Chinese Academy of Sciences, 100049, Beijing, People's Republic of China  
email: [hlyang@bao.ac.cn](mailto:hlyang@bao.ac.cn)

**Abstract.** As a relatively active region, ephemeral region (ER) exhibits highly complex pattern of magnetic flux emergence. We aim to study detailed secondary flux emergences (SFEs) which we define as bipoles that their locations close to ERs and finally coalesce with ERs after a period. We study the SFEs during the whole process from emergence to decay of 5 ERs observed by the Helioseismic and Magnetic Imager (HMI) aboard Solar Dynamics Observatory (SDO). We find that the maximum unsigned magnetic flux for each of the ERs is around  $10^{20}$  Mx. All ERs have tens of SFEs with an average emerging magnetic flux of approximately  $5 \times 10^{18}$  Mx. The frequency of normalized magnetic flux for all the SFEs follows a power law distribution with an index of -2.08. The majority of SFEs occur between the positive and negative polarities of ER, and their growth time is concentrated within one hour. The magnetic axis of SFEs also exhibits a random characteristic. We suggest that the relationship between SFEs and ERs can be understood by regarding the photospheric magnetic field observations as cross-sections of an emerging magnetic structure. Tracking the ERs' evolution, we propose that the flux emergences are partially emerged  $\Omega$ -loops, and that the SFEs in ERs may be sequent emergences from the bundle of flux tube of ERs.

**Keywords.** Sun: Solar Magnetic Field, Sun: Magnetic Bipolarity, Sun: Magnetic Flux, Sun: Solar Activity Effects, Sun: Atmospheric heating, Sun: Magnetic Signatures, Sun: Network Analysis

---

## 1. Introduction

Ephemeral regions (ERs) are small, magnetic bipolar configurations on the surface of the Sun. During the emergence phase, their polarities tend to separate from each other, while in the later stages, they either approach and cancel, or separate and diffuse. The average total flux of a single ER is approximately  $10^{20}$  Mx, and they are not biased towards or away from active regions, making them observable at any time during the solar cycle at nearly any position (Harvey and Martin (1973)). This smallest ER appears to consist of a single bipole, although it has been reported that larger-scale ones are composed of a series of bipoles that emerge next to the original ones simultaneously and persistently (Martin (1990)).

Inspired by Martin's concept (Martin (1990)), we have analyzed five typical ephemeral regions observed by HMI aboard SDO and discovered that the bipolar configurations of ephemeral regions do not evolve regularly by growing individually from small to large and eventually disappearing. Each region consists of tens of bipolar emergences, making the phenomenon more complex than previously thought. We define the regions that occupy the vast majority of magnetic flux and exhibit slow and visually discernible topological changes as main polarities, and define these bipolar emergences as secondary flux

**Table 1.** Mean value for 5 epemeral regions

ER #	$\Phi_{\text{peak}}^{\text{ER}}$ ( $10^{20}\text{Mx}$ )	Duration (h)	Number of SFEs	$\Phi_i^{\text{SFE}}$ ( $10^{18}\text{Mx}$ )	$\sum \Phi_i^{\text{SFE}}$ ( $10^{20}\text{Mx}$ )	$\Phi_i^{\text{SFE}}/\Phi_{\text{peak}}^{\text{ER}}$	$T_{\text{gro}}$ (h)	$d_i$ ( $10^3\text{km}$ )	D ( $10^3\text{km}$ )
ER1	1.4	69.0	39	0.6-14.6	1.2	0.5%-10%	0.025-5.3	1.1-17.6	18
ER2	1.6	46.0	20	1.0-15.7	1.2	0.6%-10%	0.075-2.1	2.5-15.7	16
ER3	2.1	70.0	41	1.0-40.0	2.2	0.5%-20%	0.1-4.2	0.6-19.5	16
ER4	0.6	30.0	21	0.5-13.0	0.8	0.8%-20%	0.05-1.5	0.5-14.3	12
ER5	2.1	29.0	51	1.3-26.0	2.2	0.6%-10%	0.025-7.6	1.3-28.8	20

*Notes:*

Several average features of the studied SFEs. Specifically,  $\Phi_{\text{peak}}^{\text{ER}}$  denotes the peak magnetic flux of the corresponding ER, while  $\sum \Phi_i^{\text{SFE}}$  indicates the total magnetic flux  $\Phi_i^{\text{SFE}}$  for each of these ERs. Additionally, we report the growth time  $T_{\text{gro}}$  and the distance  $d_i$  between each SFE and its corresponding ER, as well as the range of magnetic flux  $\Phi_i^{\text{SFE}}$  for the SFEs. Finally, we also provide the maximum separation distance D of the corresponding ER bipole

emergences (SFEs), which are small bipoles that arise close to the main polarities and coalesce with them after a period of evolution and eventually become indistinguishable. In this article, we attempt to address several questions concerning ERs: the number of SFEs, their contribution to the overall ER magnetic flux, their association with the main polarities, the mechanisms of their generation, and their roles in triggering small-scale solar activities. We propose a potential sub-photospheric magnetic field configuration of  $\Omega$ -shaped loops by analyzing magnetograms over time.

## 2. Observation and Data Analysis

SDO/HMI measures line-of-sight magnetic fields at the solar photosphere using the 6173 Å Fe 1 absorption line. The pixel size is 0.5". The noise level is estimated to be around 7 Gauss per pixel, which is determined by fitting the magnetic flux density to a Gaussian distribution (Hagenaar (2001); Liu et al. (2004); Jin et al. (2011, 2020)). We select five cases of ERs for nearly four days' observation from November 20, 2010, 13:00:00 UT, to November 24, 2010, 07:00:00 UT. They are far away from existing large-scale magnetic structures and active regions. Furthermore, they are located around the disk center and exhibit a complete evolution process. To counteract the effect of differential rotation, all magnetograms are derotated to fixed positions. To improve the signal-to-noise ratio and accurately capture SFEs, we use a sequence of continuous magnetograms with a cadence of 45 seconds and apply a temporal smoothing technique by averaging images of the three preceding frames, the current frame, and the subsequent three frames, as well as a spatial smoothing technique through overlay averaging with a 2-pixel radius.

## 3. Results

*Flux distribution:* Table 1 presents the basic properties of SFEs for five ERs. First, the unsigned magnetic flux of the five ERs is approximately  $10^{20}$  Mx; Secondly, the values of  $\Phi_i^{\text{SFE}}$  (magnetic flux of each SFE) range from  $10^{17}$  to  $10^{19}$  Mx. Furthermore, for each ER, the larger the peak magnetic flux ( $\Phi_{\text{peak}}^{\text{ER}}$ ) of the ER, the stronger the upper limit of individual magnetic flux for SFE ( $\Phi_i^{\text{SFE}}$ ). We find that the peak magnetic flux of an ER is not positively correlated with the number of SFEs. For example, ER1 has a smaller  $\Phi_{\text{peak}}^{\text{ER}}$  compared to ER2, yet it exhibits a higher number of SFEs. This could be attributed to the stronger magnetic field strength of ER2, which counteracts the extent of disruption caused by turbulent convection (Cheung and Isobe (2014)).

Another intriguing observation is that according to Table 1, we observe that  $\sum \Phi_i^{\text{SFE}}$  is comparable to  $\Phi_{\text{peak}}^{\text{ER}}$ , and in some cases like ER3, ER4, and ER5,  $\sum \Phi_i^{\text{SFE}}$  exceeds  $\Phi_{\text{peak}}^{\text{ER}}$ . This implies that seemingly inconspicuous SFEs contribute to the majority of the magnetic flux in ER. In other words, ER is essentially composed of these smaller magnetic flux

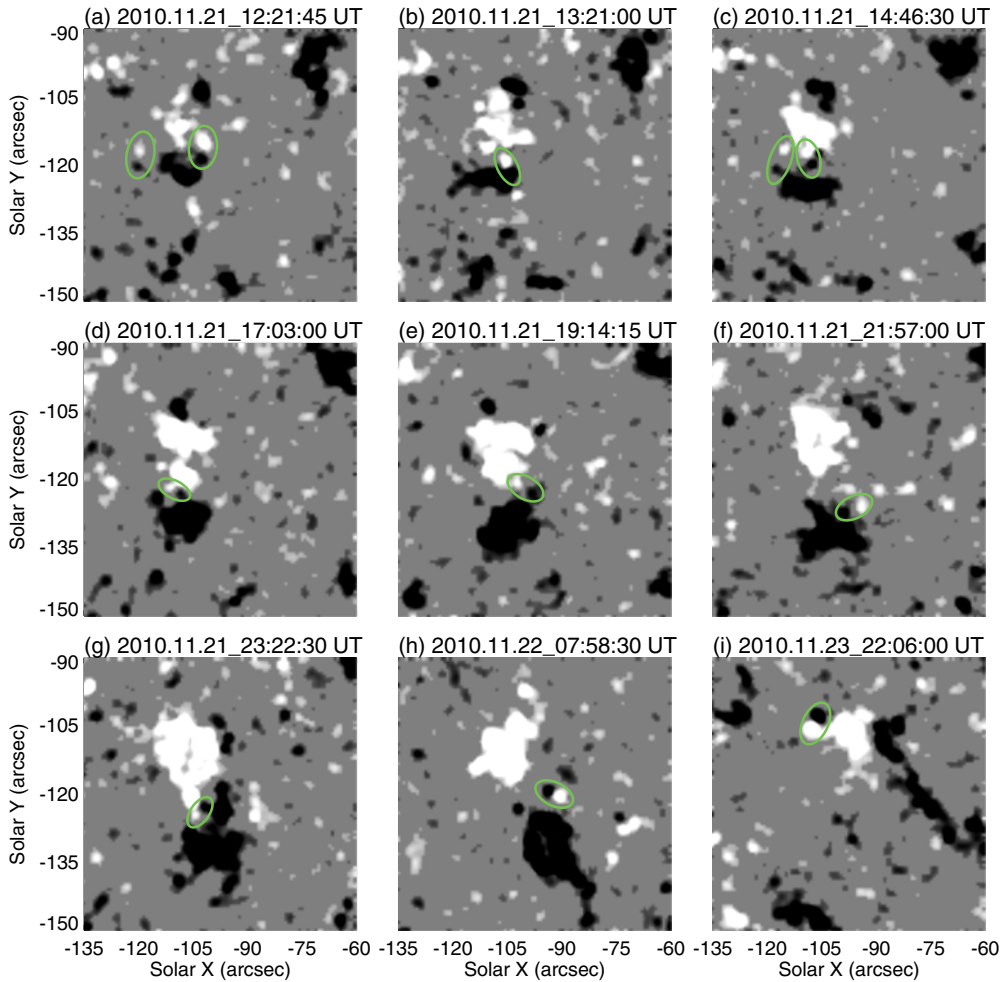


**Figure 1.** Nine representative instances of secondary flux emergence, all of which are extracted from ER1 due to its location in a relatively quiescent environment and displaying typical ER characteristics (Harvey and Martin 1973). Magnetograms reveal that SFE may arise on all sides surrounding the main bipole. As shown in panels (a)–(h), most of the SFEs eventually merge with the main polarities. However, for a small fraction of SFEs, such as the example in panel (i), magnetic cancellation is the ultimate outcome. To enhance visual contrast, we set pixel values below the noise level ( $\pm 7$  Gauss) to zero. The magnetograms saturate at  $\pm 21$  Gauss.

tubes converging. The situation where  $\sum \Phi_i^{\text{SFE}}$  surpasses  $\Phi_{\text{peak}}^{\text{ER}}$  can be attributed to the following three factors. First, SFEs do not all reach their peak strength simultaneously. When we determine the moment of peak strength in ER, some SFEs might not have emerged or reached their maximum strength. Consequently, summing each  $\Phi_i^{\text{SFE}}$  results in a magnetic flux larger than the overall flux measured at a specific time. The second point involves that, with the onset of flux cancellation, the magnetic flux in the main polarities diminishes and subsequently undergoes fragmentation (Furusawa and Sakai (1999)), giving rise to SFEs in its proximity. Consequently, flux cancellation also leads to a decrease in  $\Phi_{\text{peak}}^{\text{ER}}$  and contributes to  $\sum \Phi_i^{\text{SFE}}$ . Thirdly, during the emergence of magnetic flux tubes, deformations can occur. If split flux tubes emerge on the photosphere in the form of twisted structures, it essentially leads to repeated statistical counting. This is also responsible for the higher value of  $\sum \Phi_i^{\text{SFE}}$ .

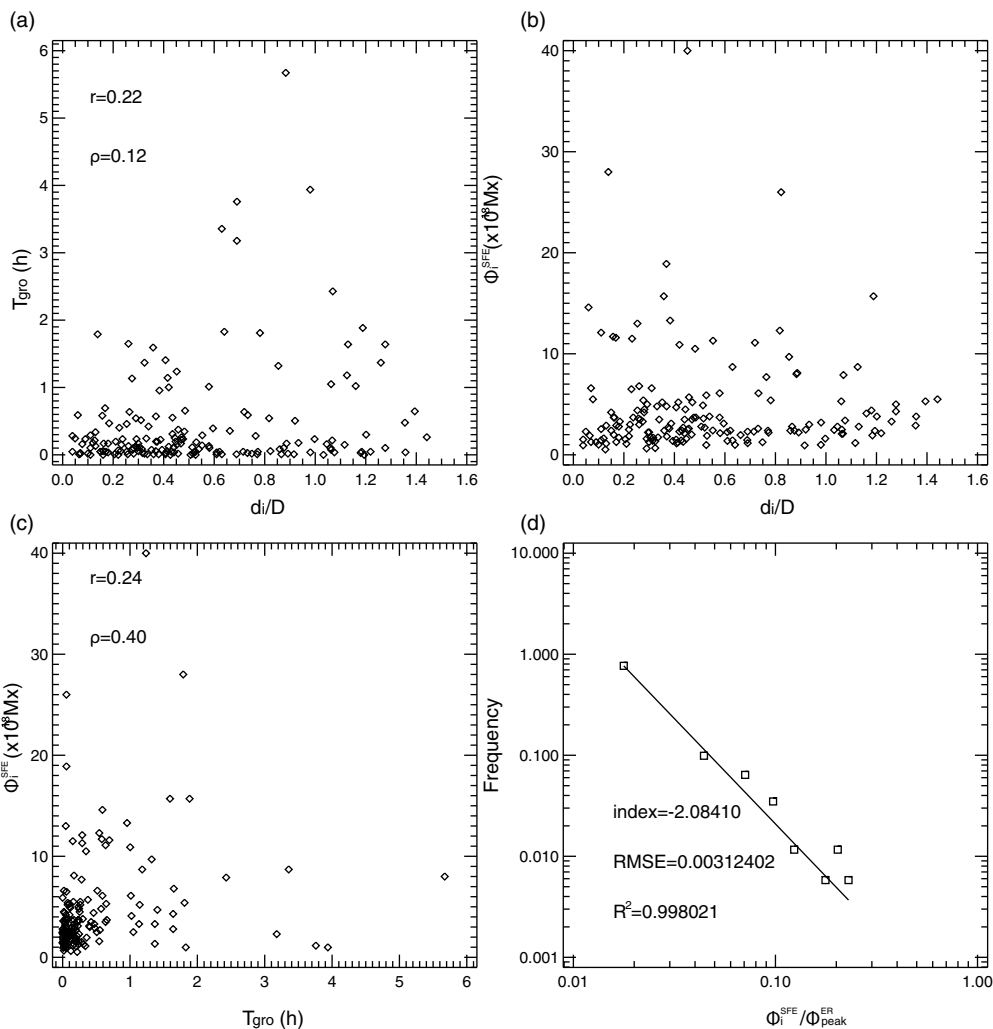


**Figure 2.** Scattered distributions of  $T_{\text{gro}}-d_i/D$ ,  $\Phi_i^{\text{SFE}}-d_i/D$ , and  $\Phi_i^{\text{SFE}}-T_{\text{gro}}$  in panel a, b, c and logarithmic coordinate frequency distribution of  $\Phi_i^{\text{SFE}}/\Phi_{\text{peak}}^{\text{ER}}$  in panel d where we employ a bin size of 0.03

If we normalize each  $\Phi_i^{\text{SFE}}$  by the  $\Phi_{\text{peak}}^{\text{ER}}$  of its corresponding ER and construct their frequency distribution, we observe that this distribution approximately conforms to a power law. Therefore, we perform a power-law fitting of the data points. After logarithmic transformation of the x and y coordinates, we plot the data points along with the fitted curve in panel d of Figure 2. We employ nine bins, with one bin having a frequency of 0. Due to the occurrence of mathematical errors caused by logarithmic transformation, only eight points are indicated on the graph. Our calculations yield an index of approximately -2.08. To gauge the goodness of fit, we compute the coefficient of determination ( $R^2$ ) and the root mean square error (RMSE). The resulting values are 0.998 and 0.003, respectively, indicating that the distribution of the relative strength of SFE, i.e.,  $\Phi_i^{\text{SFE}}/\Phi_{\text{peak}}^{\text{ER}}$ , is likely to conform to a power-law distribution with an index of -2.08.

*Growth time:* Table 1 shows SFEs'  $T_{\text{gro}}$  (growth time) of 5 ERs. Most SFEs grow to their maximum or merge into the main polarities and lose their identities within an hour or even several minutes. However, there are also a few SFEs that maintain their

independence even after several mergers and separations from the main polarities. After a long period, they may take several hours to reach their maximum. From panels a and c in Figure 2, it can be observed that there are instances of  $T_{\text{gro}}$  extending over several hours. Some undergo multiple mergers at the same location, while others remain stationary for prolonged periods with negligible changes. Additionally, certain SFEs maintain a low magnetic level for a period before undergoing a sudden enhancement, rapidly merging into main polarities. These occurrences are situated on the periphery of panel a and c. This could be due to their relatively larger distance from the main polarities, allowing us to observe their independent evolutions for a longer period, thereby enabling us to derive their peak strengths from a broader time range. Furthermore, we calculate the Pearson correlation coefficient  $r$  (0.22 in panel a, 0.24 in panel c) and the Spearman correlation coefficient  $\rho$  (0.12 in panel a, 0.40 in panel c) for  $d_i/D - T_{\text{gro}}$  and  $T_{\text{gro}} - \Phi_i^{\text{SFE}}$ , revealing that in the case of our 172 SFE samples, there is no apparent linear correlation between these parameters. The stochastic behavior indicates that, in the majority of common scenarios, a normal distribution and correlation can be identified between  $T_{\text{gro}}$  and  $\Phi_i^{\text{SFE}}$  (if eliminating biases introduced by the definition of  $T_{\text{gro}}$ ). Although panel c appears to exhibit no discernible correlation, this could be attributed to the impact of the enhanced scale generated by large values of  $T_{\text{gro}}$ . Moreover, prolonged growth does not necessarily result in stronger magnetic flux. In specific cases, we can observe that certain SFEs can reach flux exceeding  $10^{19}$  Mx within minutes, while others may grow for a longer period without significantly stronger magnetic flux than most SFEs. This could be attributed to the inherent strength of the magnetic flux tube branch, determining the strength of SFE. Some branches exhibit fast growth, while others grow more slowly. However, the growth time does not fundamentally dictate the amount of magnetic flux involved in SFEs.

*Orientation:* Figure 3 depicts all SFEs marked with arrows in the same plot. The color bar ranging from purple to red represents the chronological sequence of SFEs. The direction of the arrow points from the positive to the negative polarities. When the magnetic flux of the ER reaches its initial state, peak state, and dissipation state, the arrows connecting the magnetic centroids are marked more prominently in the figure with thicker lines. It can be observed that in the early stage of evolution, SFE tends to appear more often in the middle of the two main polarities. Whereas in the later phase, SFE tends to appear more diffusely around ERs. Another characteristic is that SFEs with larger angles between their magnetic axes and ER's tend to appear around the periphery of main polarities. Conversely, SFEs between the main polarities exhibit seldom large angles. The reason behind this phenomenon might be similar to the aforementioned point. For smaller branches, they are susceptible to distortion or deformation due to drag from turbulent convection during the emergence, resulting in structures such as kinks and twists (this will be discussed in detail in the next section). When they emerge with an inclination, their magnetic axes exhibit larger angles with the magnetic axis of the ER. In contrast, stronger SFEs are better equipped to resist turbulent convection and maintain their shape, allowing them to emerge closer to main polarities, that is, in the middle region between main polarities. After emergence, SFEs naturally follow the rotation of the ERs, but their initial deviations do not align with with the rotational trend of the ER.

#### 4. Discussion

This study presents a detailed investigation of the secondary flux emergence (SFE) process in ephemeral regions (ERs), based on observations of the line-of-sight (LOS) magnetic field obtained from HMI/SDO. Using a visual inspection method, 39, 23, 43, 21, and 48 SFEs are identified in five selected ERs, which is much higher in quantity than previously studies. The magnetic flux of the five ERs is  $1.4 \times 10^{20}$  Mx,  $1.6 \times 10^{20}$  Mx,  $2.1 \times 10^{20}$  Mx,  $0.6 \times 10^{20}$  Mx, and  $\times 10^{20}$  Mx, respectively. The magnetic flux of SFEs

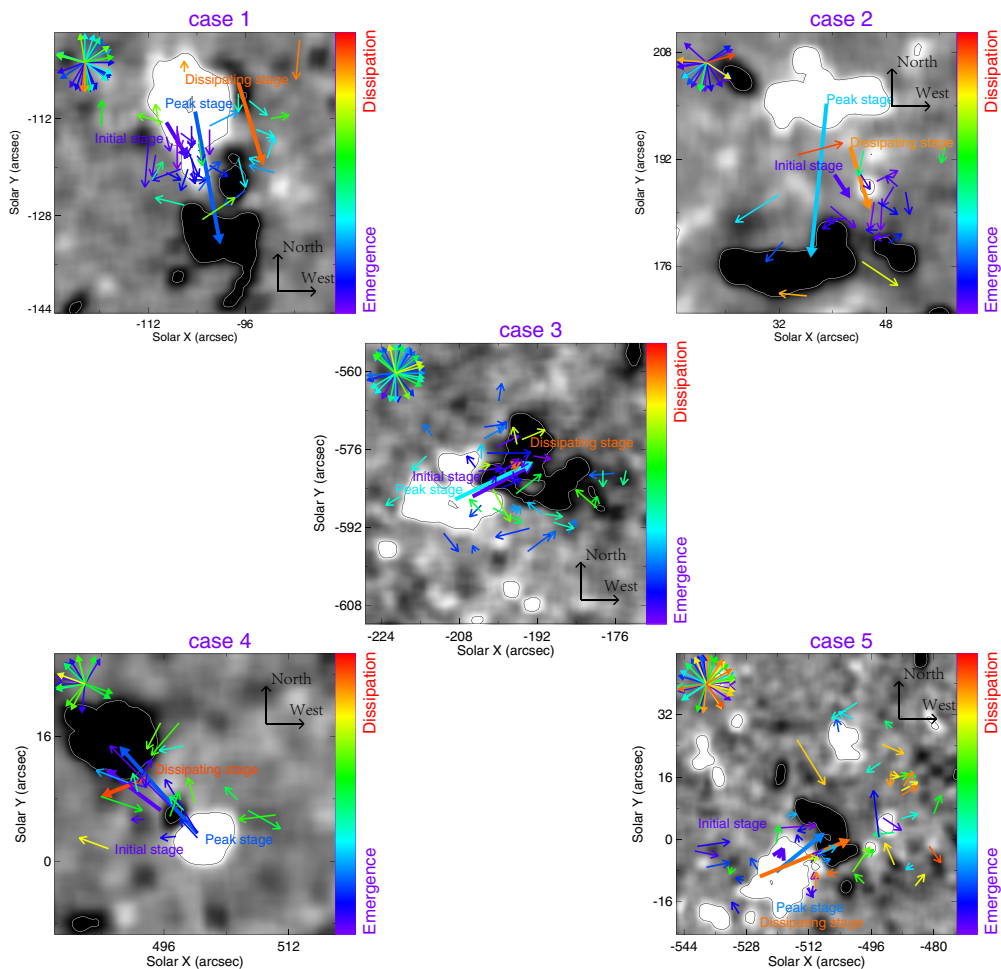


**Figure 3.** All SFEs with main polarities of ERs marked in magnetograms using arrows. Five magnetograms are selected at the time of maximum magnetic flux for their respective ERs and contour lines with a value of 21 Gauss are used. The arrows start and end at the positive and negative polarities of the SFEs, respectively. The color indicates the time of SFEs' birth according to the color bar. The main polarities positions during the initial, peak, and dissipation phases are also marked with thick arrows. The arrows in the top left corner of each image represent the direction distribution of SFEs within concentric circles.

relative to their corresponding ER flux follows a power law distribution with an index of  $-2.08$ . Previous studies on flux emergence at different scales (from intranetwork to active regions) suggests a power law with an index of  $-1.85$  (Parnell et al. 2009). We attribute this scale-free phenomenon to the influence of near-surface turbulent convection, causing the magnetic flux tubes to systematically break down into a power-law distribution, spanning various scales of magnetic flux emergence. Some studies propose that this might originate from a scale-free dynamo, yet further theoretical and observational validation is required to confirm this hypothesis (Thornton and Parnell (2011)).

Our observations suggest that the ERs are manifestations of the emergence of partially emerged magnetic flux loops from the photosphere, while the SFEs are smaller loops from the corresponding ER structures, as shown in Figure 4. Based on the tracking of the SFEs in the magnetogram, it can be inferred that magnetic flux tubes may exhibit not

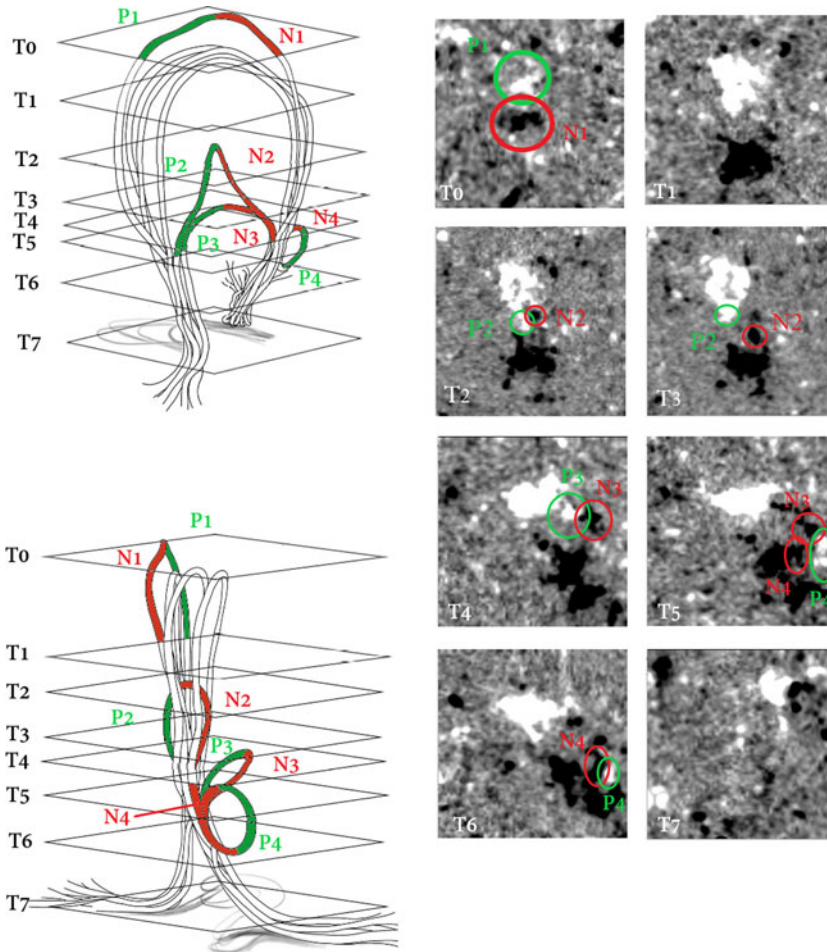


**Figure 4.** Front and side views of magnetic field configurations of the emerging magnetic flux derived from a series of consecutive magnetograms from ER1. The magnetograms spanning from 21-Nov 11:58:30 UT to 21-Nov 21:27:00 UT for T0 to T1, 21-Nov 22:42:45 UT to 22-Nov 01:08:15 UT for T2 to T3, 22-Nov 10:56:15 UT to 22-Nov 14:25:30 UT for T4 to T6 and 24-Nov 00:04:30 UT for T7 are displayed to construct a schematic for subsurface structures. The left part showcases the positive polarities P1, P2, P3, and P4 in green, while the negative polarities are denoted as N1, N2, N3, and N4 in red. The magnetograms on the right part simultaneously label the corresponding positive and negative polarities of each SFE using green and red circles, respectively.

only regular arch structures, but also various types of twisted and distorted shapes (such as P2, N2, P4, N4). As illustrated in Figure 4, when the magnetic flux tube is below the photosphere, it is tightly confined by the high-density plasma (Longcope and Welsch (2000)). As it rises, the gas pressure decreases, causing some magnetic flux tube branches to detach from the main tube and emerge independently. Since they separate from the same hosting magnetic tube, as the emergence continues, the branches eventually rejoin the loop, demonstrating the connection between the SFE and ER. The frequency distribution of the normalized flux of SFEs reflects the nature that the magnetic flux tube scatters under the influence of turbulent convection. The growth time and distance from the ER represent the emergence rate and the actual coverage range of the ER, respectively. The rotation observed in ER reflects a slight twist of the magnetic flux tube.

## References

- Cheung, M. C. M. & Isobe, H. 2014, *Living Reviews in Solar Physics*, 11, 3.
- Furusawa, K. & Sakai, J.-I. 1999.
- Hagenaar, H. J. 2001, *Astrophys. J.*, 555, 448–461.
- Harvey, K. L. & Martin, S. F. 1973, *Solar Physics*, 32, 389–402.
- Jin, C., Zhou, G., Zhang, Y., & Wang, J. 2020, *Astrophys. J. Lett.*, 889, L26.
- Jin, C. L., Wang, J. X., Song, Q., & Zhao, H. 2011, *Astrophys. J.*, 731, 37.
- Liu, Y., Zhao, X., & Hoeksema, J. T. 2004, *Solar Phys.*, 219, 39–53.
- Longcope, D. W. & Welsch, B. T. 2000, *Astrophys. J.*, 545, 1089–1100.
- Martin, S. F. 1990, *Memorie della Societa Astronomica Italiana*, 61, 293–315.
- Parnell, C. E., DeForest, C. E., Hagenaar, H. J., Johnston, B. A., Lamb, D. A., & Welsch, B. T. 2009, *Astrophys. J.*, 698, 75–82.
- Schrijver, C. J., Title, A. M., Harvey, K. L., Sheeley, N. R., Wang, Y. M., van den Oord, G. H. J., Shine, R. A., Tarbell, T. D., & Hurlburt, N. E. 1998, *Nature*, 394, 152–154.
- Thornton, L. M. & Parnell, C. E. 2011, *Solar Phys.*, 269, 13–40.